Available online at www.sciencedirect.com
ScienceDirect
International Journal of Heat and Mass Transfer 50 (2007) 3990–4002
International Journal of HEAT and MASS TRANSFER
www.elsevier.com/locate/ijhmt

Visualizing energy flows through energy streamlines and pathlines

Shohel Mahmud *, Roydon Andrew Fraser

Department of Mechanical Engineering, University of Waterloo, 200 University Avenue West, Waterloo, Ont., Canada N2L3G1

Received 26 February 2006; received in revised form 26 January 2007
Available online 28 March 2007

Abstract

This paper describes the new technique of *total* energy flow visualization inside channels and enclosures for natural, mixed, and forced convection heat transfer problems. Specifically, the flow of the total energy is visualized by energy streamlines or pathlines. In 2-D, energy streamlines are obtained by solving a Poisson equation of type $\nabla^2\Phi = (\nabla \times \dot{\mathbf{E}}) \cdot \hat{k}$ where Φ is the energy streamfunction. $\dot{\mathbf{E}}$ is the energy flux density vector and $\hat{k}$ is the unit vector. One of the objectives of this paper is to find expressions for $\dot{\mathbf{E}}$ as a function of velocity, temperature, electric field, magnetic field, and fluid/flow properties. In 3-D, energy pathlines are used to visualize total energy flow. In concept, "total energy" includes all relevant forms of energy; for example, thermal, potential, kinetic, magnetic, electrical, and chemical. Steady-state convection heat transfer problems are selected from the available literature and energy streamlines are presented for these problems. For unsteady periodic problems, energy streamfunctions are calculated from the time averaged velocity, temperature, and other relevant properties. Finally, an energy pathline visualization technique is proposed for 3-D problems.

1. Introduction

It is traditional practice to use streamlines and isothermal lines together to describe flow field and thermal field characteristics, respectively, in convection heat transfer problems. Streamfunction and streamlines are very efficient and largely used tools to visualize two-dimensional flow fields [1,2]. Streamlines and isotherms, however, do not visually describe relationships between the energy flow mechanisms of fluid flow and thermal diffusion in convection problems. Combining thermal diffusion and enthalpy flows, Kimura and Bejan [3] and Bejan [4] proposed "heatline" as a powerful alternative way to visualize thermal energy flow. Heatlines simultaneously consider both conducted and convected thermal energies. In the limit of vanishingly small convective flow, the heatline reduces to the heat flux line which is a well established concept in conduction heat transfer [2]. The concept of "heatline" has been employed by other researchers to describe other situations; for example, see Ho and Lin [5], Morega and Bejan [6,7], Aggarwal and Manhapra [8], and Costa [9,10]. Furthermore, the heatline concept has recently been adapted to convective mass transfer by introducing the massfunction and massline concepts [9–13].

The objective of this paper is to introduce the energy streamline as an alternate convection heat transfer energy visualization technique. Energy streamlines as considered in this paper consider all forms of relevant energy; for example, thermal energy, potential energy, kinetic energy, electrical energy, magnetic energy, and chemical energy. An essential requirement for calculating energy streamfunctions (Φ) is to first formulate the energy flux density vector ($\dot{\mathbf{E}}$). The energy flux density vector also includes all forms of relevant energy as mentioned above and some specific forms of $\dot{\mathbf{E}}$ are derived in Sections 2–4. For a specific convection heat transfer problem, the energy streamfunction can be calculated by solving the following differential equation:

$$\frac{\partial^2\Phi}{\partial x^2} + \frac{\partial^2\Phi}{\partial y^2} = -(\nabla \times \dot{\mathbf{E}}) \cdot \hat{k} = \frac{\partial \dot{E}_x}{\partial y} - \frac{\partial \dot{E}_y}{\partial x} \tag{1}$$

* Corresponding author. Tel.: +1 519 888 4567x3885; fax: +1 519 888 6197.
E-mail address: smahmud@uwaterloo.ca (S. Mahmud).

0017-9310/$ - see front matter © 2007 Elsevier Ltd. All rights reserved.
doi:10.1016/j.ijheatmasstransfer.2007.01.032

Nomenclature

$\mathbf{B}$	magnetic induction vector, Wb m^{-2}
B_y	component of the magnetic induction vector at y direction, Wb m^{-2}
D	a reference distance, m
e	internal energy per unit mass, J kg^{-1}
E	energy per unit volume, J m^{-3}
$\mathbf{E}$	electric field intensity vector, Volt m^{-1}
$\dot{\mathbf{E}}$	energy flux density vector, W m^{-2}
Ec	Eckert number, $= u_0^2/C_p\Delta T$
$\dot{E}_x$	x component of the energy flux density vector, W m^{-2}
$\dot{E}_y$	y component of the energy flux density vector, W m^{-2}
$\dot{E}_z$	z component of the energy flux density vector, W m^{-2}
h	enthalpy per unit mass, J kg^{-1}
Ha	Hartmann number, $= B_y\sqrt{\sigma K/\mu}$
$\mathbf{J}$	current density vector, amp m^{-2}
k	thermal conductivity, W m^{-1} K^{-1}
K	permeability of the porous medium, m^2
$\hat{\mathbf{k}}$	unit vector in z direction
Pe	Péclet number, $= Re \times Pr$
Pr	Prandtl number, $= \mu/C_pk$
Ra	Rayleigh number, $= g\beta\Delta TD^3/v\alpha$
Ra_K	Darcy modified Rayleigh number, $= g\beta\Delta TDK/\alpha v$
Re	Reynolds number, $= \rho u_0 D/\mu$
s	specific entropy, J kg^{-1} K^{-1}
$\mathbf{S}$	surface vector, m^2
t	time, s
T	temperature, K
T_{ref}	a problem dependent [22–33] reference temperature, K
u_0	a problem dependent [22–33] reference velocity, m s^{-1}
$\mathbf{v}$	velocity vector, m s^{-1}

Greek symbols

ρ	density of the fluid, kg m^{-3}
σ	electric conductivity of the fluid, Ω^{-1} m^{-1}
$\boldsymbol{\sigma}$	viscous stress tensor, N m^{-2}
$\boldsymbol{\sigma}^*$	dimensionless viscous stress tensor
v	kinematic viscosity of the fluid, m^2 s^{-1}
μ	dynamic viscosity of the fluid, N s m^{-2}
μ_0	permeability of the free space, $= 4\pi \times 10^{-7}$ Wb amp^{-1} m^{-1}
Φ	energy stream function, W m^{-1}
Θ	dimensionless temperature, $= (T - T_{\text{ref}})/\Delta T$
ΔT	a problem dependent [22–33] reference temperature difference, K
$\forall$	volume, m^3

where E_x and E_y are the x and y components of the energy flux density vector ($\dot{\mathbf{E}}$) and $\hat{k}$ is the unit vector at the z direction. The application of a proper boundary condition for Eq. (1) is a complicated issue. An excellent discussion on a boundary condition for the heatline/massline equation (similar to Eq. (1)) is available in Costa [13] (see Section 2.2 of [13]). A similar argument to that considered by Costa [13] is used in the present study with the corresponding boundary condition for Eq. (1) being

$$\Phi_{\text{P,b}} = \Phi_{\text{ref,b}} + \int_{\text{ref,b}}^{\text{P,b}} \dot{\mathbf{E}}.\hat{\mathbf{n}}\,\mathrm{d}s_{\text{b}} \tag{2}$$

where subscripts '*b*', 'ref', and '*P*' represent a boundary value, a reference value, and a particular point on the boundary, respectively. $\mathrm{d}s_{\text{b}}$ is a small boundary segment whose surface normal is represented by $\hat{\mathbf{n}}$.

The term "energy streamline" has been used before by Chapman [14] to describe the energy flows associated with waves based on an energy velocity concept; energy velocity is defined as the ratio of energy flux transmitted by the wave to the energy density of the wave [14]. In contrast to the Chapman energy velocity definition of energy streamline the energy flux definition of energy streamline presented in this paper is capable of being applied to electromagnetic waves [14]. Furthermore, the energy velocity definition looses physical meaning when extended to describe conduction energy transfer. In short, energy velocity energy streamlines and energy flux energy streamlines are two distinctly different definitions for energy streamlines. To emphasise the more general nature of the energy flux energy streamline presented in this paper the authors propose that they be called *total* energy streamlines if confusion is possible.

The rest of the paper has the following format: In Section 2, an expression for $\dot{\mathbf{E}}$ is derived for a viscous fluid exposed to a temperature gradient. The expression of $\dot{\mathbf{E}}$ derived in Section 2 is extended in Section 3 to consider an external magnetic energy source. Some special cases are discussed in Section 4. Section 5 gives some graphical examples of energy streamline distribution patterns inside channels and enclosures whose streamlines and isothermal lines are available in different published articles. Section 6 describes a way to handle unsteady problems. Finally, Section 7 presents the concept of energy pathlines to visualize 3-D problems as energy streamlines are restricted to 2-D visualization.

2. Viscous fluid energy streamline

Consider a volume element fixed in space. The energy in this unit volume of the fluid is

$$E = \frac{1}{2}\rho v^2 + \rho e; \quad (v^2 = |\mathbf{v}|^2 = u_x^2 + u_y^2 + u_z^2) \tag{3}$$

where the first term on the right hand side is the kinetic energy and the second term is the internal energy per unit volume, respectively. In Eq. (3), e is the internal energy per unit mass. The rate of change in E with time is given by the following partial derivative

$$\frac{\partial E}{\partial t} = \frac{\partial}{\partial t}\left(\frac{1}{2}\rho v^2 + \rho e\right). \tag{4}$$

In order to calculate the quantity $\partial E/\partial t$, the right hand side of Eq. (4) can be expanded to

$$\frac{\partial}{\partial t}\left(\frac{1}{2}\rho v^2 + \rho e\right) = \frac{1}{2}v^2\frac{\partial \rho}{\partial t} + \rho\mathbf{v}\cdot\frac{\partial \mathbf{v}}{\partial t} + \rho\frac{\partial e}{\partial t} + e\frac{\partial \rho}{\partial t}. \tag{5}$$

The four consecutive terms on the right hand side of Eq. (5) are calculated next. Using the continuity equation [1],

$$\frac{\partial \rho}{\partial t} + \nabla\cdot(\rho\mathbf{v}) = 0, \tag{6}$$

the first term can be expressed as

$$\frac{1}{2}v^2\frac{\partial \rho}{\partial t} = -\frac{1}{2}v^2\nabla\cdot(\rho\mathbf{v}). \tag{7}$$

Using the Navier–Stokes equation without gravity [15],

$$\frac{\partial \mathbf{v}}{\partial t} + (\mathbf{v}\cdot\nabla)\mathbf{v} = -\frac{1}{\rho}\nabla p + \frac{1}{\rho}\frac{\partial \sigma'_{ik}}{\partial x_k}, \tag{8}$$

the second term of Eq. (5) can be expressed as

$$\rho\mathbf{v}\cdot\frac{\partial \mathbf{v}}{\partial t} = -\rho\mathbf{v}\cdot(\mathbf{v}\cdot\nabla)\mathbf{v} - \mathbf{v}\cdot\nabla p + \mathbf{v}\cdot\frac{\partial \sigma'_{ik}}{\partial x_k}. \tag{9}$$

In Eqs. (8) and (9), σ'_{ik} is the *viscous stress tensor* which imparts the irreversible "viscous" transfer of momentum from the fluid. Following Bird et al. [15] and Landau and Lifshitz [16], σ'_{ik} can be expressed as

$$\sigma'_{ik} = \mu\left(\frac{\partial v_i}{\partial x_k} + \frac{\partial v_k}{\partial x_i} - \frac{2}{3}\delta_{ik}\frac{\partial v_j}{\partial x_j}\right) + \varsigma\delta_{ik}\frac{\partial v_j}{\partial x_j} \tag{10}$$

where μ, ζ, and δ_{ik} are the dynamic (or absolute) viscosity of the fluid, bulk (or second) viscosity of the fluid, and Kronecker delta, respectively. A vector transformation of the $\mathbf{v}\cdot(\mathbf{v}\cdot\nabla)\mathbf{v}$ term in Eq. (9) yields [15]:

$$\mathbf{v}\cdot(\mathbf{v}\cdot\nabla)\mathbf{v} = \frac{1}{2}\mathbf{v}\cdot\nabla(v^2). \tag{11}$$

Next, using the following thermodynamic relation, $\mathrm{d}h = T\mathrm{d}s + \mathrm{d}p/\rho$ [17], ∇p in Eq. (9) can be transformed into the following form:

$$\nabla p = \rho\nabla h - \rho T\nabla s \tag{12}$$

where h and s are the enthalpy and entropy per unit mass, respectively. The last term on the right hand side of Eq. (9) can be transformed to

$$\begin{aligned}\mathbf{v}\cdot\frac{\partial \sigma'_{ik}}{\partial x_k} &= v_i\frac{\partial \sigma'_{ik}}{\partial x_k} = \frac{\partial}{\partial x_k}\left(v_i\sigma'_{ik}\right) - \sigma'_{ik}\frac{\partial v_i}{\partial x_k}\\ &= \nabla\cdot(\mathbf{v}\cdot\boldsymbol{\sigma}) - \sigma'_{ik}\frac{\partial v_i}{\partial x_k}\end{aligned} \tag{13}$$

where $\mathbf{v}\cdot\boldsymbol{\sigma}$ denotes the vector whose components are $v_i\sigma'_{ik}$ [15]. Using Eqs. (11)–(13), (9) becomes

$$\begin{aligned}\rho\mathbf{v}\cdot\frac{\partial \mathbf{v}}{\partial t} = &-\frac{1}{2}\rho\mathbf{v}\cdot\nabla(v^2) - \rho\mathbf{v}.\nabla h + \rho T\mathbf{v}\cdot\nabla s\\ &+ \nabla\cdot(\mathbf{v}\cdot\boldsymbol{\sigma}) - \sigma'_{ik}\frac{\partial v_i}{\partial x_k}.\end{aligned} \tag{14}$$

Using the thermodynamic relation [17]

$$\mathrm{d}e = T\mathrm{d}s - p\mathrm{d}\forall = T\mathrm{d}s + \frac{p}{\rho^2}\mathrm{d}\rho, \tag{15}$$

the third term on the right hand side of Eq. (5) can be expressed as

$$\rho\frac{\partial e}{\partial t} = \rho\left(T\frac{\partial s}{\partial t} + \frac{p}{\rho^2}\frac{\partial \rho}{\partial t}\right) = \rho T\frac{\partial s}{\partial t} - \frac{p}{\rho}\nabla\cdot(\rho\mathbf{v}), \tag{16}$$

where the continuity equation (Eq. (6)) is used to obtain the final form of Eq. (16). Using these transformations, Eq. (5) can be expressed as

$$\begin{aligned}\frac{\partial}{\partial t}\left(\frac{1}{2}\rho v^2 + \rho e\right) = &-\frac{1}{2}v^2\nabla\cdot(\rho\mathbf{v}) - \frac{1}{2}\rho\mathbf{v}\cdot\nabla(v^2)\\ &- \rho\mathbf{v}\cdot\nabla h + \rho T\mathbf{v}\cdot\nabla s + \nabla\cdot(\mathbf{v}\cdot\boldsymbol{\sigma})\\ &- \sigma'_{ik}\frac{\partial v_i}{\partial x_k} + \rho T\frac{\partial s}{\partial t} - \frac{p}{\rho}\nabla\cdot(\rho\mathbf{v}) - e\nabla\cdot(\rho\mathbf{v}).\end{aligned} \tag{17}$$

Rearranging the right hand side of Eq. (17) one can obtain

$$\begin{aligned}\frac{\partial}{\partial t}\left(\frac{1}{2}\rho v^2 + \rho e\right) = &-\left(\frac{1}{2}v^2 + e + \frac{p}{\rho}\right)\nabla\cdot(\rho\mathbf{v})\\ &- \rho\mathbf{v}\cdot\nabla\left(\frac{1}{2}v^2 + h\right) - \nabla\cdot(k\nabla T) + \nabla\cdot(\mathbf{v}\cdot\boldsymbol{\sigma})\\ &- \sigma'_{ik}\frac{\partial v_i}{\partial x_k} + \rho T\left[\frac{\partial s}{\partial t} + \mathbf{v}\cdot\nabla s\right] + \nabla\cdot(k\nabla T).\end{aligned} \tag{18}$$

Note that the term $\nabla.(k\nabla T)$ is subtracted and added to Eq. (18), the reason for doing this is to enable clear identification of the energy equation in Eq. (23) below. Now, the thermodynamic relation [17]

$$e + \frac{p}{\rho} = h \tag{19}$$

can be used to get a more compact form of Eq. (18) as

$$\frac{\partial}{\partial t}\left(\frac{1}{2}\rho v^2+\rho e\right)=-\left(\frac{1}{2}v^2+h\right)\nabla\cdot(\rho\mathbf{v})-\rho\mathbf{v}\cdot\nabla\left(\frac{1}{2}v^2+h\right)+\nabla\cdot(k\nabla T)+\nabla\cdot(\mathbf{v}\cdot\boldsymbol{\sigma})-\sigma'_{ik}\frac{\partial v_i}{\partial x_k}+\rho T\left[\frac{\partial s}{\partial t}+\mathbf{v}\cdot\nabla s\right]-\nabla\cdot(k\nabla T). \tag{20}$$

Using the vector operation [15]

$$\nabla\cdot(a\mathbf{b})=a\nabla\cdot(\mathbf{b})+\mathbf{b}\cdot\nabla(a), \tag{21}$$

Eq. (20) can be converted into the following form:

$$\frac{\partial}{\partial t}\left(\frac{1}{2}\rho v^2+\rho e\right)=-\nabla\cdot\left[\rho\mathbf{v}\left(\frac{1}{2}v^2+h\right)\right]+\nabla\cdot(\mathbf{v}\cdot\boldsymbol{\sigma})+\nabla\cdot(k\nabla T)-\sigma'_{ik}\frac{\partial v_i}{\partial x_k}+\rho T\left[\frac{\partial s}{\partial t}+\mathbf{v}\cdot\nabla s\right]-\nabla\cdot(k\nabla T), \tag{22}$$

which, after some additional simplifications and rearrangements, becomes

$$\frac{\partial}{\partial t}\left(\frac{1}{2}\rho v^2+\rho e\right)=-\nabla\cdot\left[\rho\mathbf{v}\left(\frac{1}{2}v^2+h\right)-\mathbf{v}\cdot\boldsymbol{\sigma}-k\nabla T\right]+\rho T\left[\frac{\partial s}{\partial t}+\mathbf{v}\cdot\nabla s\right]-\nabla\cdot(k\nabla T)-\sigma'_{ik}\frac{\partial v_i}{\partial x_k}. \tag{23}$$

Finally, using the following specific form of the energy equation [16],

$$\rho T\left[\frac{\partial s}{\partial t}+\mathbf{v}\cdot\nabla s\right]=\nabla\cdot(k\nabla T)+\sigma'_{ik}\frac{\partial v_i}{\partial x_k}, \tag{24}$$

one can express Eq. (23) as

$$\frac{\partial}{\partial t}\left(\frac{1}{2}\rho v^2+\rho e\right)=-\nabla\cdot\left[\rho\mathbf{v}\left(\frac{1}{2}v^2+h\right)-\mathbf{v}\cdot\boldsymbol{\sigma}-k\nabla T\right]=-\nabla\cdot(\dot{\mathbf{E}}). \tag{25}$$

To assist in the interpretation of Eq. (25) it can be integrated over a given closed volume as follows:

$$\frac{\partial}{\partial t}\int_{\forall}\left(\frac{1}{2}\rho v^2+\rho e\right)\mathrm{d}\forall=-\int_{\forall}\nabla\cdot\left[\rho\mathbf{v}\left(\frac{1}{2}v^2+h\right)-\mathbf{v}\cdot\boldsymbol{\sigma}-k\nabla T\right]\mathrm{d}\forall=-\oint\left[\rho\mathbf{v}\left(\frac{1}{2}v^2+h\right)-\mathbf{v}\cdot\boldsymbol{\sigma}-k\nabla T\right]\cdot\mathrm{d}\mathbf{S}. \tag{26}$$

The final form of Eq. (26) is obtained after converting the volume integral to a surface integral. The left hand side of Eq. (26) is the rate of change of energy in a given volume. The right hand side is the amount of energy flowing into this volume in unit time. The negative sign on the right hand side means that the surface integral describes the energy flowing out of the given volume. With this interpretation of the surface integral, the expression

$$\dot{\mathbf{E}}=\rho\mathbf{v}\left(\frac{1}{2}v^2+h\right)-\mathbf{v}\cdot\boldsymbol{\sigma}-k\nabla T \tag{27}$$

will be called the *energy flux density* vector and it has units of energy per unit volume per unit time. In steady state, Eq. (25) reduces to

$$\nabla\cdot\dot{\mathbf{E}}=0. \tag{28}$$

Eq. (28) tells one that the steady-state energy flux density is a conserved quantity like mass flux density in an incompressible fluid. For a two-dimensional problem in Cartesian co-ordinates, the x and y components of Eq. (27) can be expressed as

$$\dot{E}_x=\rho u_x\left\{\frac{1}{2}(u_x^2+u_y^2)+h\right\}-(u_x\sigma_{xx}+u_y\sigma_{yx})-k\frac{\partial T}{\partial x} \tag{29a}$$

$$\dot{E}_y=\rho u_y\left\{\frac{1}{2}(u_x^2+u_y^2)+h\right\}-(u_x\sigma_{xy}+u_y\sigma_{yy})-k\frac{\partial T}{\partial y} \tag{29b}$$

where

$$\sigma_{xx}=\mu\frac{2}{3}\left[2\frac{\partial u_x}{\partial x}-\frac{\partial u_y}{\partial y}\right],\quad \sigma_{yy}=\mu\frac{2}{3}\left[2\frac{\partial u_y}{\partial y}-\frac{\partial u_x}{\partial x}\right],\quad \sigma_{xy}=\sigma_{yx}=\mu\left[\frac{\partial u_x}{\partial y}+\frac{\partial u_y}{\partial x}\right] \tag{30}$$

are obtained from Eq. (10) assuming a zero bulk viscosity.

3. Energy streamlines in presence of a magnetic force

In the presence of an external field (in this case a magnetic force), Eqs. (25) and (27) must be modified accordingly. A magnetic field stores energy in conducting fluids, energy that will be shown capable of flowing in or out of a given volume as a magnetic energy flux. To start, Eq. (4) must now include a magnetic energy term ($=B^2/2\mu_0$) where B and μ_0 are the magnetic induction and the permeability of free space, respectively. Therefore, the modified equation becomes

$$\frac{\partial \mathrm{E}}{\partial t}=\frac{\partial}{\partial t}\left(\frac{1}{2}\rho v^2+\rho e+\frac{B^2}{2\mu_0}\right). \tag{31}$$

After expansion, Eq. (31) becomes

$$\frac{\partial}{\partial t}\left(\frac{1}{2}\rho v^2+\rho e+\frac{B^2}{2\mu_0}\right)=\frac{1}{2}v^2\frac{\partial\rho}{\partial t}+\rho\mathbf{v}\cdot\frac{\partial\mathbf{v}}{\partial t}+\rho\frac{\partial e}{\partial t}+e\frac{\partial\rho}{\partial t}+\frac{1}{\mu_0}\mathbf{B}\cdot\frac{\partial\mathbf{B}}{\partial t}. \tag{32}$$

The first, third, and fourth terms on the right hand side of Eq. (32) have already been calculated in Eqs. (7), (16), and (17) and need no additional modification. In order to calculate the second term one needs to consider the momentum equation, including the magnetic force, as follows [18]:

$$\frac{\partial\mathbf{v}}{\partial t}+(\mathbf{v}\cdot\nabla)\mathbf{v}=-\frac{1}{\rho}\nabla p+\frac{1}{\rho}\frac{\partial\sigma'_{ik}}{\partial x_k}+\frac{1}{\rho}(\mathbf{J}\times\mathbf{B}). \tag{33}$$

Therefore, the second term on the right hand side of Eq. (32) becomes

$$\rho\mathbf{v}\cdot\frac{\partial\mathbf{v}}{\partial t}=-\rho\mathbf{v}\cdot(\mathbf{v}\cdot\nabla)\mathbf{v}-\mathbf{v}\cdot\nabla p+\mathbf{v}\cdot\frac{\partial\sigma'_{ik}}{\partial x_k}+\mathbf{v}\cdot(\mathbf{J}\times\mathbf{B}). \tag{34}$$

The first, second, and the third terms on the right hand side of Eq. (34) have already been calculated in Eqs. (11)–(13). The fourth term can be calculated as

$$\left(\rho\mathbf{v}\cdot\frac{\partial\mathbf{v}}{\partial t}\right)_{\mathrm{MHD}}=\mathbf{v}\cdot(\mathbf{J}\times\mathbf{B})=-\mathbf{J}\cdot(\mathbf{v}\times\mathbf{B}). \tag{35}$$

The $\rho\mathbf{v}\cdot\partial\mathbf{v}/\partial t$ term in Eq. (34) contains four different terms and first three of them are already calculated in Section 2. In this section, the fourth term (magnetic term) will be calculated and, for convenience, the subscript 'MHD' on the left hand side of Eq. (35) is used to represent the magnetic force component term only from Eq. (34). Using Maxwell's equation [18] $\partial\mathbf{B}/\partial t=-\nabla\times\mathbf{E}$, the fifth term on the right hand side of Eq. (32) can be written as

$$\frac{1}{\mu_0}\mathbf{B}\cdot\frac{\partial\mathbf{B}}{\partial t}=\frac{1}{\mu_0}\mathbf{B}\cdot[-\nabla\times(\mathbf{E})] \tag{36}$$

where the electric field ($\mathbf{E}$) can be approximated using Ohm's law [18], $\mathbf{J}=\sigma(\mathbf{E}+\mathbf{v}\times\mathbf{B})$, as

$$\mathbf{E}=\frac{\mathbf{J}}{\sigma}-\mathbf{v}\times\mathbf{B} \tag{37}$$

where $\mathbf{J}$ and σ are the volume current density and the electrical conductivity of the fluid, respectively. Using Eq. (37), the right hand side of Eq. (36) becomes

$$\frac{1}{\mu_0}\mathbf{B}\cdot[-\nabla\times(\mathbf{E})]=-\frac{1}{\mu_0}\mathbf{B}\cdot\left[\nabla\times\left(\frac{\mathbf{J}}{\sigma}\right)\right]+\frac{1}{\mu_0}\mathbf{B}\cdot[\nabla\times(\mathbf{v}\times\mathbf{B})]. \tag{38}$$

Using the vector identity [15] $\nabla\cdot(\mathbf{a}\times\mathbf{b})=\mathbf{b}\cdot\nabla\times\mathbf{a}-\mathbf{a}\cdot\nabla\times\mathbf{b}$, the first term on the right hand side of Eq. (38) can be expressed as (for constant μ_0 and σ)

$$\begin{aligned}\frac{1}{\mu_0}\mathbf{B}\cdot\left[\nabla\times\left(\frac{\mathbf{J}}{\sigma}\right)\right]&=\frac{1}{\sigma\mu_0}\mathbf{B}\cdot[\nabla\times(\mathbf{J})]\\&=\frac{1}{\sigma\mu_0}[\nabla\cdot(\mathbf{J}\times\mathbf{B})+\mu_0\mathbf{J}^2].\end{aligned} \tag{39}$$

And using the same vector identity, the second term on the right hand side of Eq. (38) can be written as

$$\begin{aligned}\frac{1}{\mu_0}\mathbf{B}\cdot[\nabla\times(\mathbf{v}\times\mathbf{B})]&=\frac{1}{\mu_0}\nabla\cdot[(\mathbf{v}\times\mathbf{B})\times\mathbf{B}]+\frac{1}{\mu_0}(\mathbf{v}\times\mathbf{B})\cdot\nabla\times(\mathbf{B})\\&=-\frac{1}{\mu_0}\nabla\cdot[\mathbf{B}\times(\mathbf{v}\times\mathbf{B})]+\frac{1}{\mu_0}\nabla\times(\mathbf{B})\cdot(\mathbf{v}\times\mathbf{B})\\&=-\frac{1}{\mu_0}\nabla\cdot[\mathbf{B}\times(\mathbf{v}\times\mathbf{B})]+\mathbf{J}\cdot(\mathbf{v}\times\mathbf{B})\end{aligned} \tag{40}$$

after using Maxwell's equation [18] $\nabla\times\mathbf{B}=\mu_0\mathbf{J}$. Considering Eqs. (39) and (40), (38) becomes

$$\begin{aligned}\frac{1}{\mu_0}\mathbf{B}\cdot[-\nabla\times(\mathbf{E})]=-\nabla\cdot\left(\frac{\mathbf{J}\times\mathbf{B}}{\sigma\mu_0}\right)-\frac{\mathbf{J}^2}{\sigma}-\frac{1}{\mu_0}\nabla\cdot[\mathbf{B}\times(\mathbf{v}\times\mathbf{B})]\\+\mathbf{J}\cdot(\mathbf{v}\times\mathbf{B}).\end{aligned} \tag{41}$$

Additional modifications using Eqs. (35) and (36) yields

$$\begin{aligned}&\left(\rho\mathbf{v}\cdot\frac{\partial\mathbf{v}}{\partial t}\right)_{\mathrm{MHD}}+\frac{1}{\mu_0}\mathbf{B}\cdot\frac{\partial\mathbf{B}}{\partial t}\\&\quad=-\frac{1}{\mu_0}\nabla\cdot[\mathbf{B}\times(\mathbf{v}\times\mathbf{B})]-\nabla\cdot\left(\frac{\mathbf{J}\times\mathbf{B}}{\sigma\mu_0}\right)-\frac{\mathbf{J}^2}{\sigma}.\end{aligned} \tag{42}$$

Finally, Eq. (32) becomes

$$\begin{aligned}\frac{\partial}{\partial t}\left(\frac{1}{2}\rho v^2+\rho e+\frac{B^2}{2\mu_0}\right)=-\nabla\cdot\Bigg[\rho\mathbf{v}\left(\frac{1}{2}v^2+h\right)-\mathbf{v}\cdot\boldsymbol{\sigma}-k\nabla T\\+\frac{1}{\sigma\mu_0}(\mathbf{J}\times\mathbf{B})+\frac{1}{\mu_0}[\mathbf{B}\times(\mathbf{v}\times\mathbf{B})]\Bigg]\\+\rho T\left[\frac{\partial s}{\partial t}+\mathbf{v}.\nabla s\right]-\nabla.(k\nabla T)-\sigma'_{ik}\frac{\partial v_i}{\partial x_k}-\frac{\mathbf{J}^2}{\sigma}\end{aligned} \tag{43}$$

where $\mathbf{J}^2/\sigma$ is Joule dissipation [18,19]. Using the following specific form of the energy equation [16],

$$\rho T\left[\frac{\partial s}{\partial t}+\mathbf{v}\cdot\nabla s\right]=\nabla\cdot(k\nabla T)+\sigma'_{ik}\frac{\partial v_i}{\partial x_k}+\frac{\mathbf{J}^2}{\sigma}, \tag{44}$$

the *energy flux density* vector including magnetic energy becomes

$$\begin{aligned}\dot{\mathbf{E}}=\rho\mathbf{v}\left(\frac{1}{2}v^2+h\right)-\mathbf{v}.\boldsymbol{\sigma}-k\nabla T+\frac{1}{\sigma\mu_0}(\mathbf{J}\times\mathbf{B})\\+\frac{1}{\mu_0}[\mathbf{B}\times(\mathbf{v}\times\mathbf{B})].\end{aligned} \tag{45}$$

Eq. (45) is the required expression for the energy flux density vector in the presence of a magnetic field.

4. Extending the energy flux density vector to other cases

The derived expressions for the energy flux densities given by Eq. (27) and extended by Eq. (45) to magnetic fields can be further extended to describe porous media, gravitational energy, and other forms of energy. For each case, one needs to identify the additional source term(s) in the energy and momentum conservation equations, and to consider the modified thermodynamic relations due to those source terms.

4.1. Porous media

Consider convective flow through a porous medium. If one considers, for example, the Darcy–Brinkman–Forchheimer model of porous medium [20,21], the Darcy term $(\nu/K)\mathbf{v}$ and the Forchheimer term $(C/\sqrt{K})\mathbf{v}|\mathbf{v}|$ in the momentum equation [20,21] result in two additional terms, $\rho(\nu/K)\mathbf{v}\cdot\mathbf{v}$ and $\rho(C/\sqrt{K})\mathbf{v}\cdot\mathbf{v}|\mathbf{v}|$, on the right hand side of Eq. (9). These two additional terms are represented by the viscous dissipation function

$$\Phi_{\text{diss}} = \left(\frac{\mu}{K} + \frac{\rho C}{\sqrt{K}}|\mathbf{v}|\right)\mathbf{v}\cdot\mathbf{v} \tag{46}$$

in the energy equation for porous medium [21]. Therefore, the form of the energy flux density equation for porous medium is similar to Eq. (27) but velocity and temperature should be read as volume averaged velocity and volume averaged temperature, and the thermophysical properties should be read as the effective thermophysical properties of porous media [4].

4.2. Gravitational energy

Consider, next, the effect of gravity. As mentioned in Landau and Lifshitz [16], the effect of gravity on energy flux density is negligible unless the system considered is very large. The energy inherent to gravitational force is the potential energy $\rho\,\mathbf{r}\cdot\mathbf{g}$ [16] where $\mathbf{r}$ and $\mathbf{g}$ are the position and gravity vectors, respectively. For a large system, the $\rho\,\mathbf{r}\cdot\mathbf{g}$ term should be placed inside the time derivative on the right hand side of Eq. (4). The momentum equation (Eq. (8)) must have a gravity source term $\mathbf{g}$ added to the right hand side. If it is assumed that the gravity field is independent of time, then one needs to calculate two additional terms; that is, $(\mathbf{r}\cdot\mathbf{g})\partial\rho/\partial t$ and $\rho\,\mathbf{v}\cdot\mathbf{g}$. Considering the product $\mathbf{r}\cdot\mathbf{g}$ as a gravity potential φ [16], the gravity vector $\mathbf{g}$ can be expressed as $-\nabla\varphi$[16] which enables the terms $(\mathbf{r}\cdot\mathbf{g})\partial\rho/\partial t$ and $\rho\,\mathbf{v}\cdot\mathbf{g}$ to be expressed as

$$(\mathbf{r}\cdot\mathbf{g})\frac{\partial\rho}{\partial t} = -\varphi\nabla\cdot(\rho\mathbf{v}) \quad \text{and} \quad \rho\,\mathbf{v}\cdot\mathbf{g} = -\rho\mathbf{v}\cdot\nabla\varphi. \tag{47}$$

Performing similar mathematical operations to those used to obtain in Eqs. (17)–(23), one can finally express the gravity force modified energy flux density equation for a large system with an unchanging gravity field as

$$\dot{\mathbf{E}} = \rho\mathbf{v}\left(\frac{1}{2}v^2 + h + \varphi\right) - \mathbf{v}\cdot\boldsymbol{\sigma} - k\nabla T. \tag{48}$$

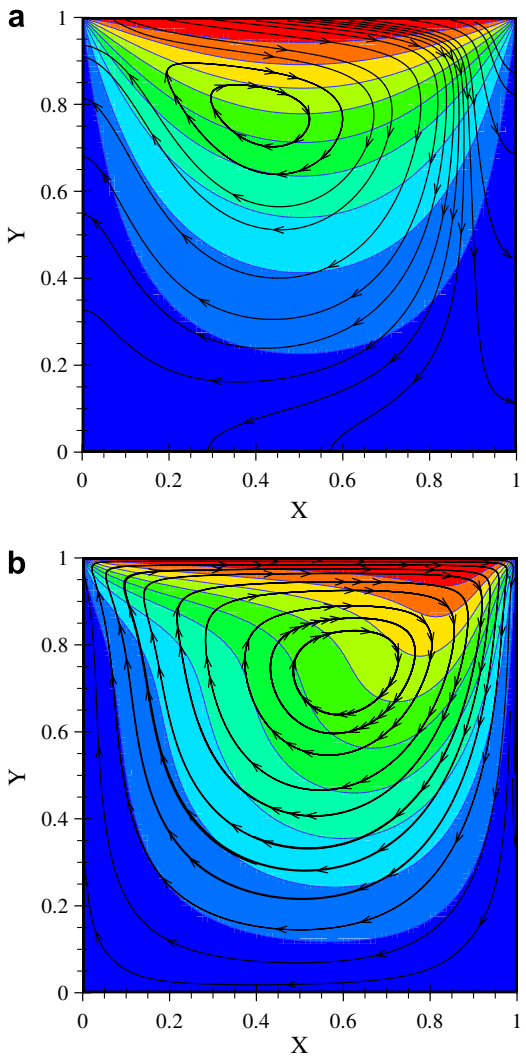

Fig. 1. Lid driven cavity flow at (a) $Re = 1$ and (b) $Re = 100$.

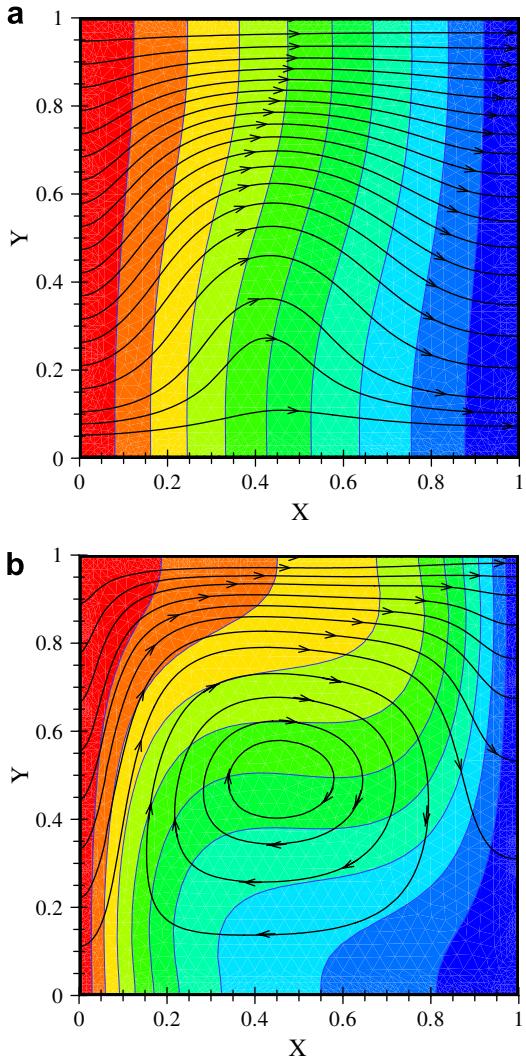

Fig. 2. Buoyancy induced flow in a square cavity at (a) $Ra = 5 \times 10^2$ and (b) $Ra = 1 \times 10^4$.

5. Examples in 2-D

In this section, several 2-D problems are selected from the available literature [22–33] to show the associated energy streamline distribution pattern. The selection of 2-D test cases is arbitrary. Only steady-state and 2-D problems are discussed in this section. The discussions on unsteady and 3-D problems are left for the following two sections. For each test case, the governing momentum and energy equations are numerically solved using a finite volume method. A detail description of the method, discretization scheme, and solution algorithm is available in Hortmann et al. [22] and is not repeated here. However, it should be noted that many other problems available in the heat transfer literature [34–54] are well suited for such analysis.

The contribution of different energy components (the right hand side of Eqs. (27), (45), or Eq. (48)) on energy flux density (as well as on energy streamfunction) largely depends on the fluid, flow, and geometric properties for a particular convection heat transfer problem. In order to observe the influence of these energy components, Eq. (27) is cast into non-dimensional form for the cases of either forced or natural convection yielding

Forced convection:

$$\dot{\mathbf{E}}/E_0 = Ec\,Pe\left[\mathbf{V}\frac{1}{2}|\mathbf{V}|^2\right] - Ec\,Pr\mathbf{V}\cdot\sigma^* + Pe(\mathbf{V}\Theta) - \nabla\Theta \tag{49a}$$

Natural convection:

$$\dot{\mathbf{E}}/\mathrm{E}_0 = Ec\,Ra\left[\mathbf{V}\frac{1}{2}|\mathbf{V}|^2\right] - Ec\,Pr\mathbf{V}\cdot\sigma^* + Ra(\mathbf{V}\Theta) - \nabla\Theta \tag{49b}$$

where E_0 is a reference energy flux density ($= k\Delta T/W$) and Ra, Pe, and Ec are the Rayleigh number, Péclet number, and Eckert number, respectively, as defined in the nomenclature section. In order to obtain Eqs. (49a) and (49b), characteristics of velocity and temperature, as described in references [22–33], are used. Since there are cases where each of the terms on the right hand side of Eqs. (49a) and (49b) can be zero the choice of energy flux for non-dimensionalization purposes was based on the fact that this work focuses on heat transfer problems. That is, heat transfer implies the presence of a non-zero temperature gradient and hence there will always be a non-zero magnitude to the reference energy flux. The choice of reference temperature difference (ΔT) is problem dependent [22–33]. It is observed from Eqs. (49a) and (49b) that the relative magnitudes of the different energy components also depend on the magnitudes of Ra, Pe, and Ec.

Hot walls always act as one of the sources of energy streamlines. Similarly, cold walls always act as one of the sinks of energy streamlines. At a vanishingly small Péclet number ($Pe \approx 0$) or relatively low Rayleigh number, where the velocity components are very small the contribution of kinetic energy and convective thermal energy is negligible compared to that of conductive thermal energy. As mentioned earlier, energy streamlines become heat flux lines at very small Ra or Pe. As such, at low Ra or Pe essentially all the "free" energy streamlines originate at the hot wall, pass through the fluid, and intersect the cold wall. For a closed system an energy streamline is said to be "free" that originates at the hot wall or other energy source, passes through the fluid, and terminates at the cold wall or other energy sink, while one that originates inside the fluid region and forms a closed loop is said to be "trapped". When Ra or Pe is relatively high, kinetic energy and convective ther-

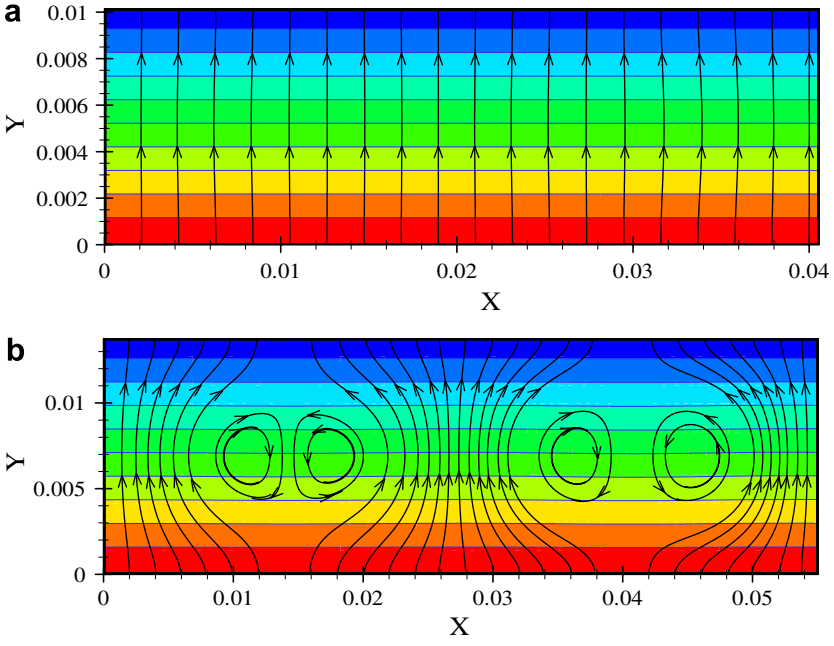

Fig. 3. The Rayleigh–Benard convection at (a) $Ra = 1000$ and (b) $Ra = 2500$.

mal energy dominate and the "trapped" energy streamlines occupy a large portion of the channel or cavity. In forced convection, the "trapped" energy streamlines occupy a major portion of the channel or cavity even at low Péclet number.

As the first example, consider lid driven cavity flow [23,24] in a square enclosure. Fig. 1a and b display the energy streamlines for Reynolds number $Re = 1$ and 100, respectively. The top wall in Fig. 1 is hot and is moving from left to right while the remaining three walls are cold and stationary. Reynolds number is calculated based on the lid velocity (u_0) and cavity height or width (D). Ten isothermal lines with uniform ΔT are additionally plotted in each figure. The arrow-marks in each energy streamline indicate its direction.

The next example is the classical buoyancy induced natural convection in a square cavity problem [22]. Energy streamlines and isothermal lines for $Ra = 5 \times 10^2$ and 1×10^4 are displayed in Fig. 2a and b, respectively. The definition of Ra is given in the nomenclature. In Fig. 2, the two vertical walls are isothermal but the temperature of the left wall is higher than the right wall, while the top and bottom walls are thermally insulated.

The third example is Rayleigh–Bénard convection [25] in an enclosure of aspect ratio 0.25 (=height/width). The Rayleigh number for this case is defined based on the height of the cavity. Fig. 3a and b display the energy streamlines and isothermal lines for $Ra = 1000$ and $Ra = 2500$, respectively. In Fig. 3, the two horizontal walls are isothermal but the temperature of the bottom wall is higher than the top wall, while the left and right walls are thermally insulated.

In order to show the energy streamline patterns inside a complicated geometry a wavy enclosure under free convection [26] is selected as the fourth example. The energy streamlines and isothermal lines are displayed in Fig. 4a and b for $Ra = 5 \times 10^2$ and $Ra = 1 \times 10^4$, respectively. The Rayleigh number is calculated based on the average

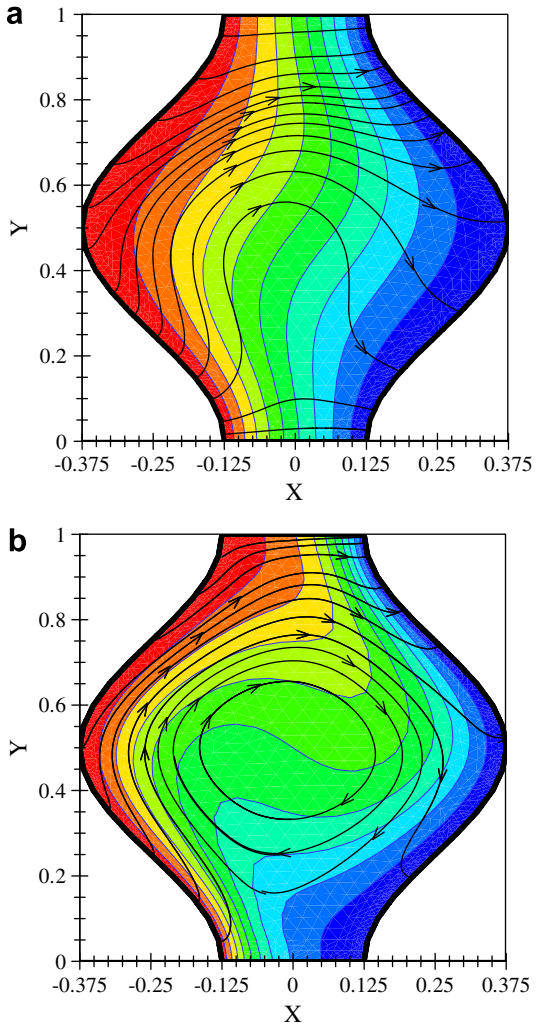

Fig. 4. Free convection inside a wavy cavity at (a) $Ra = 5 \times 10^2$ and (b) $Ra = 1 \times 10^4$.

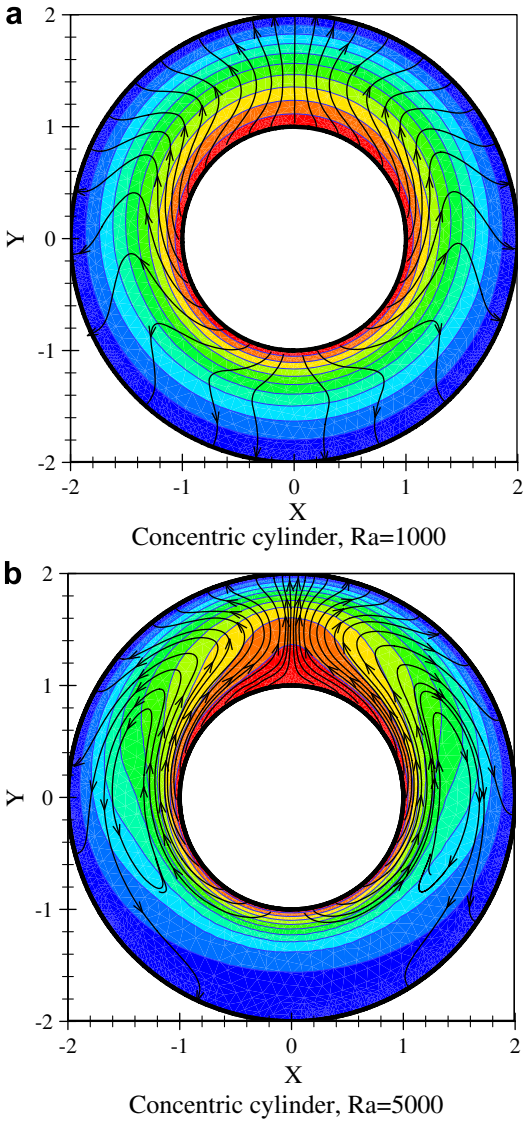

Fig. 5. Free convection inside a concentric annular space at (a) $Ra = 10^3$ and (b) $Ra = 5 \times 10^3$.

interwall spacing of the wavy walls [26]. The enclosure height to average interwall spacing ratio is kept equal to 2. In Fig. 4, the two wavy walls are isothermal but the temperature of the left wavy wall is higher than the right wavy wall, while the top and bottom walls are thermally insulated.

In the fifth example, natural convection heat transfer is considered inside a concentric annular space [27]. Fig. 5a and b show the energy streamlines and isothermal lines at $Ra = 10^3$ and 5×10^3, respectively. Rayleigh number is calculated based on $(r_o - r_i)$ where r_o and r_i are the outer radius and inner radius, respectively. In Fig. 5, both cylinders are isothermal but the inner cylinder is hot and the outer cylinder is cold.

In the sixth example, a more complicated case of finned surface or baffled surface under natural convection is considered. Recent studies of Shi and Khodadadi [28] and Tasnim and Collins [29] present the complex fluid dynamics and heat transfer characteristics of cavities with fins or baffles attached to the hot wall as shown in Fig. 6. For $Ra = 10^3$ and 5×10^3. Fig. 6a and b show the energy streamlines and isothermal lines inside a finned or baffled cavity. Rayleigh number is calculated based on the height of the cavity. The temperature of the left wall with the fin (or baffle) is higher than the temperatures of the remaining three walls.

In the seventh example, both porous medium and magnetic force are considered together. A square cavity filled with a porous medium under natural convection [4,30] is considered to be one of the classic problems of convection. At Darcy modified Rayleigh number, $Ra_K = 100$, Fig. 7a shows the distributions of the energy streamlines and isothermal lines inside the cavity. The definition of Ra_K is available in the nomenclature section. A magnetic field can modify the flow and thermal fields [31,32] of such a cavity flow significantly. Corresponding energy streamlines and isothermal lines are displayed in Fig. 7b for a $Ra_K = 100$ and $Ha = 5$, where Ha is the Hartmann number

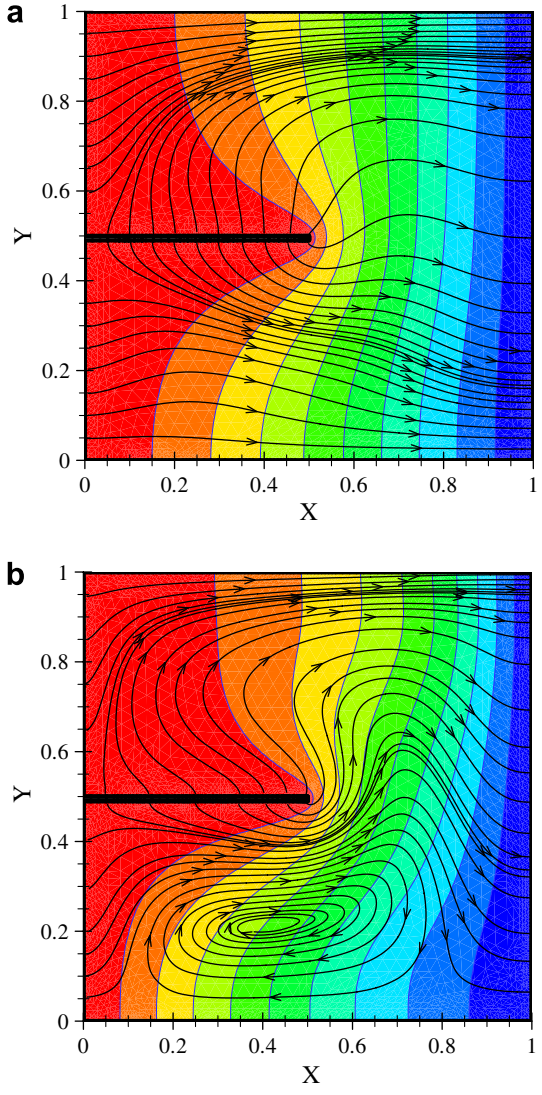

Fig. 6. Free convection in a cavity with fin or baffle at (a) $Ra = 10^3$ and (b) $Ra = 5 \times 10^3$.

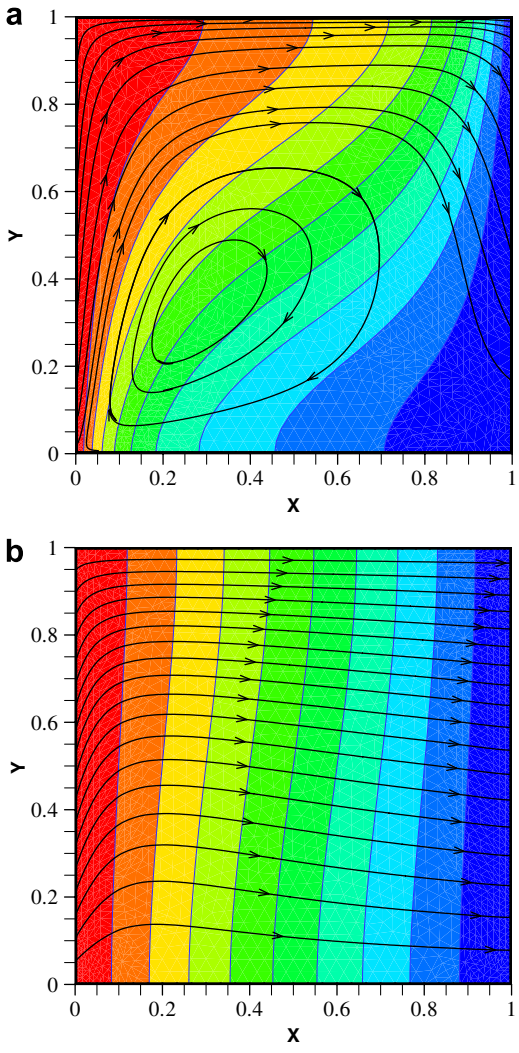

Fig. 7. Free convection in a porous cavity with transverse magnetic field at (a) $Ra = 100$ and $Ha = 0$ and (b) $Ra = 100$, $Ha = 5$.

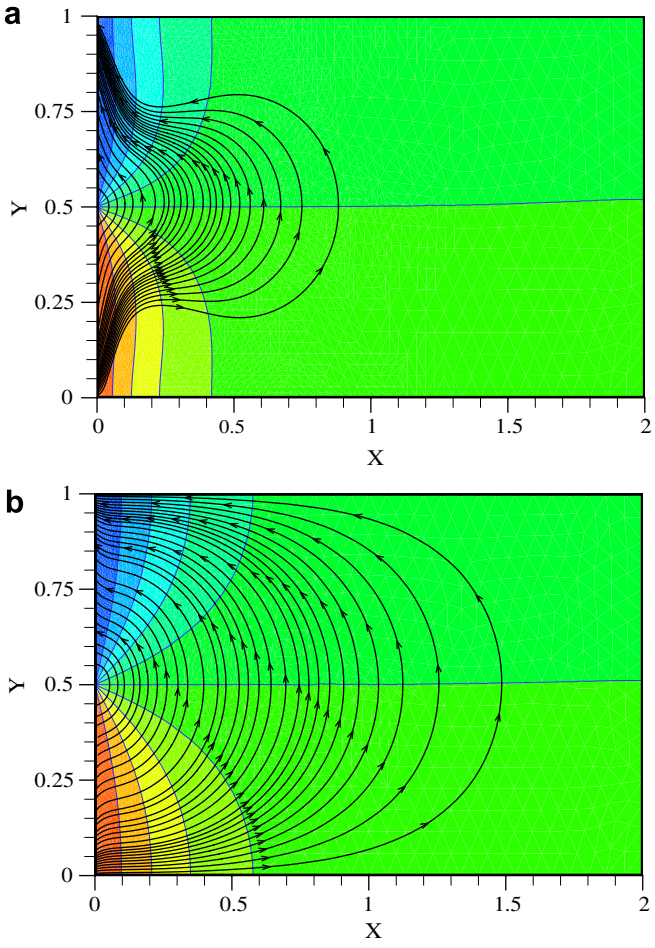

Fig. 8. Penetrative convection with hot bottom and cold top at (a) $Ra = 50$, $Ha = 0$ and (b) $Ra = 50$, $Ha = 5$.

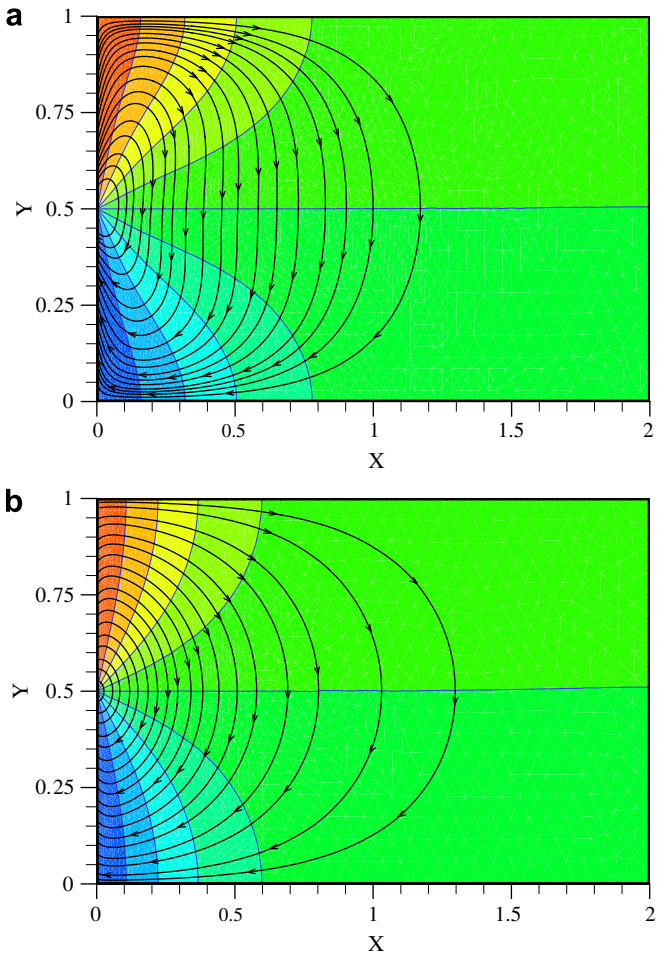

Fig. 9. Penetrative convection with hot top and cold bottom at (a) $Ra = 50$, $Ha = 0$ and (b) $Ra = 50$, $Ha = 5$.

(see nomenclature for definition) which is the ratio of the magnetic force to the viscous force.

The eighth and ninth examples are shown in Figs. 8 and 9 where penetrative convection in a porous layer [33] is considered for two different orientations of the hot and cold walls. In Fig. 8, the bottom half of the left isothermal wall is hot, while the top half is cold (complete penetration [33]). In Fig. 9, the bottom half of the left isothermal wall is cold, while the top half is hot (incomplete penetration [33]). The remaining three walls in Figs. 8 and 9 are thermally insulated. The Darcy modified Rayleigh number is calculated based on the height of the cavity. Figs. 8a and 9a show the energy streamlines and isothermal lines for $Ra_K = 50$ and $Ha = 0$, while Figs. 8b and 9b show the energy streamlines and isothermal lines for $Ra_K = 50$ and $Ha = 5$.

6. Unsteady periodic problem in 2-D

For time dependent periodic problems, the energy streamfunction can be estimated from the time averaged energy flux density vector. One good example of such a problem is the thermoacoustic effect as found in thermoacoustic engines and refrigerators [55]. For temporally periodic problems like that found in thermoacoustic engines and refrigerators, the time average over one or multiple time periods of Eq. (25) leads to

$$\frac{1}{\tau}\int_0^\tau \frac{\partial}{\partial t}\left(\frac{1}{2}\rho v^2 + \rho e\right)\mathrm{d}\tau = 0; \quad \text{with } \tau = \frac{2\pi}{\omega} \tag{50}$$

where ω is the angular frequency of oscillation. In such a case, the time averaged energy flux density vector becomes

$$\frac{1}{\tau}\int_0^\tau \dot{\mathbf{E}}\mathrm{d}\tau = \bar{\dot{\mathbf{E}}} = \overline{\rho\mathbf{v}\left(\frac{1}{2}v^2 + h\right)} - \overline{\mathbf{v}\cdot\boldsymbol{\sigma}} - \overline{k\nabla T} \tag{51}$$

where the overbar denotes the time average of a variable or expression. For different thermoacoustic problems in 2-D, Cao et al. [56], Ishikawa and Mee [57], and Mahmud and Fraser [58] calculate and display the energy flux density near a thermoacoustic stack. Fig. 10 shows an example of an energy streamline distribution near a thermoacoustic stack.

7. Problems in 3-D

The concept of streamfunction, mass function, heat function, and energy streamfunction is invalid for 3-D

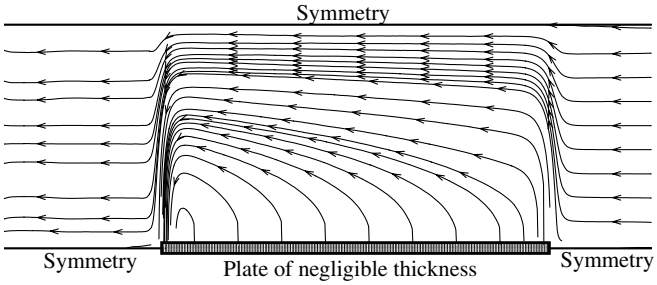

Fig. 10. The energy streamline near a stack plate of negligible thickness. Helium is the working fluid. Properties of helium are calculated at $T_m = 298.15$ K. Other input parameters are DR = 1.7%, $\omega = 628.571$ rad/s, $S_w = 2.45$, $Pr = 0.6672$, and $\lambda = 10.1595$ m. The domain length (DL) equals $\lambda/4$ and the plate length (L) equals 5% of λ. The outer edge (here right side) of the plate is located at one-eighth of the λ.

problems because of the definitions of such functions are restricted to 2-D. Although Mallinson and Davis [59] claim to display streamlines in a 3-D box under natural convection, these lines are actually streaklines or pathlines as presented and discussed by many authors; for example, Bednarz et al. [60]. Bednarz et al. [60] report experimental results with numerical verification of natural convection flow and thermal fields in a cube in a magnetic field. In order to show the energy flow in a 3-D problem, the three components ($\dot{E}_x$, $\dot{E}_y$, and $\dot{E}_z$) of the energy flux density vector are calculated from the converged results of velocity and temperature. These three components are used to trace an imaginary path of energy flow similar to the pathline trace that is seen in references [59,60]. For demonstration purposes, the special 3-D case of natural convection inside a differentially heated cubical cavity is selected for $Ra = 10^3$. The commercial code StarCD/StarWorks [61] are used to calculate the flow and thermal fields results. The hot and cold walls of the cavity are shown in Fig. 11a with the remaining walls thermally insulated. Fig. 11a and b show the "free" energy pathline originating at the middle portion and lower portion of the hot wall, passing through the fluid, and terminating at the cold wall. Two energy pathlines are shown in Fig. 11c and d where, for each case, the energy pathline originates at the hot wall (the point of origin is indicated by a filled circle at the hot wall), makes complicated spiral loops inside the fluid region, and finally terminate at the cold wall (the point of termination is indicated by a filled circle at the cold wall).

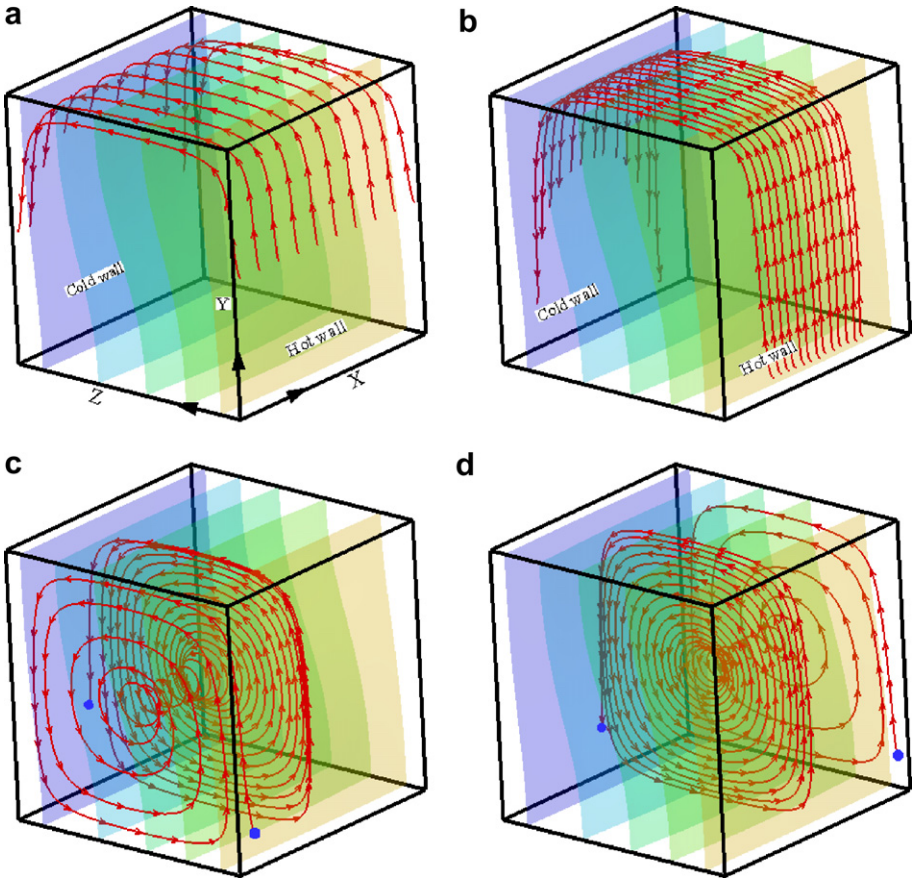

Fig. 11. Energy streaklines in a 3-D cubical cavity under natural convection at $Ra = 10^3$. (a) 10 equidistance energy streaklines from the middle of the hot wall ($X = 0$ to 1, $Y = 0.5$, and $Z = 0$), (b) 13 equidistance energy streaklines from the lower part of the hot wall ($X = 0.25$ to 0.75, $Y = 0.05$, and $Z = 0$), (c) one energy streakline from the lower part of the hot wall ($X = 0.1$, $Y = 0.2$, and $Z = 0$), and (d) one energy streakline from the lower part of the hot wall ($X = 0.9$, $Y = 0.2$, and $Z = 0$).

8. Conclusions

The main objective of this paper is to propose the new method of energy streamlines to visualize total energy flows in convective heat transfer problems. This new approach is analogous to the use of "streamfunctions" and "streamlines" to visualize fluid flow; "heatfunctions" and "heatlines" to visualize combined conductive–convective thermal energy flow; and "massfunctions" and "masslines" to visualize mass flow, but with a focus on total energy flow. An expression for the energy flux density vector is calculated in order to solve a Poisson type equation for the energy streamline. The magnitude of this energy flux density vector is equal to the amount of energy passing, in unit time, through a unit area. The energy streamline distribution pattern for a particular problem depends on the transport property Péclet number (forced convection) or Rayleigh number (natural convection). Hot walls always act as sources while cold walls act as sinks for energy streamlines. An energy streamline is said to be "free" that originates at the hot wall, passes through the fluid, and terminates at the cold wall, while one that originates inside the fluid region and forms a closed loop is said to be "trapped". As expected, for a vanishingly small velocity ($Pe \to 0$ or $Ra \to 0$), the energy streamline simplifies to the heat flux line. For a negligible kinetic energy ($Ec \to 0$), the energy streamline simplifies to the heatline in the absence of any external or internal source of energy. As for unsteady problems, the energy streamfunction can be calculated from the time averaged energy flux density vector, and as for 3-D problems, the concept of energy streamlines is replaced by energy pathlines.

References

[1] F.M. White, Viscous Fluid Flow, McGraw-Hill, New York, 1991.
[2] E.R.G. Eckert, R.M. Drake Jr., Analysis of Heat and Mass Transfer, McGraw-Hill, New York, 1972.
[3] S. Kimura, A. Bejan, The "heatline" visualization of convective heat transfer, J. Heat Transfer 105 (1983) 916–919.
[4] A. Bejan, Convection Heat Transfer, Wiley, New York, 1984.
[5] C.J. Ho, Y.H. Lin, Natural convection of cold water in a vertical annulus with constant heat flux on the inner wall, J. Heat Transfer 112 (1990) 117–123.
[6] A.M. Morega, A. Bejan, Heatline visualization of forced convection boundary layers, Int. J. Heat Mass Transfer 36 (1993) 3957–3966.
[7] A.M. Morega, A. Bejan, Heatline visualization of forced convection in porous media, Int. J. Heat Fluid Flow 15 (1994) 42–47.
[8] S.K. Aggarwal, A. Manhapra, Use of heatlines for unsteady buoyancy-driven flow in a cylindrical enclosure, J. Heat Transfer 111 (1989) 576–578.
[9] V.A.F. Costa, Unification of the streamline, heatline and massline methods for the visualization of two-dimensional transport phenomena, Int. J. Heat Mass Transfer 42 (1999) 27–33.
[10] V.A.F. Costa, Unification of the streamline, heatline and massline methods for the visualization of two-dimensional heat and mass transfer in anisotropic media, Int. J. Heat Mass Transfer 46 (2003) 1309–1320.
[11] O.V. Trevisan, A. Bejan, Combined heat and mass transfer by natural convection in a vertical enclosure, J. Heat Transfer 109 (1987) 104–112.
[12] V.A.F. Costa, Double diffusive natural convection in a square enclosure with heat and mass diffusive walls, Int. J. Heat Mass Transfer 40 (1997) 4061–4071.
[13] V.A.F. Costa, Bejan's heatlines and masslines for convection visualization and analysis, Appl. Mech. Rev. 59 (2006) 126–145.
[14] C.J. Chapman, Energy paths in edge waves, J. Fluid Mech. 426 (2001) 135–154.
[15] R.B. Bird, W.E. Stewart, E.N. Lightfoot, Transport Phenomena, second ed., Wiley, New York, 2002.
[16] L.D. Landau, E.M. Lifshitz, Fluid Mechanics, Pergamon Press, New York, 1982.
[17] Y.A. Çengel, M.A. Boles, Thermodynamics: An Engineering Approach, third ed., McGraw-Hill, New York, 1998.
[18] P.A. Davidson, An Introduction to Magnetohydrodynamics, Cambridge University Press, Cambridge, 2001.
[19] L.D. Landau, E.M. Lifshitz, Electrodynamics of Continuous Media, Pergamon Press, New York, 1984.
[20] D.A. Nield, A. Bejan, Convection in Porous Media, second ed., Springer-Verlag, New York, 1999.
[21] L.C. Burmeister, Convective Heat Transfer, second ed., Wiley, New York, 1993.
[22] M. Hortmann, M. Peric, G. Scheuerer, Finite volume multigrid prediction of laminar natural convection: Bench-mark solutions, Int. J. Numer. Methods Fluids 11 (1990) 189–207.
[23] O.R. Burggraf, Analytical and numerical studies of the structure of steady separated flows, J. Fluid Mech. 24 (1966) 113–151.
[24] U. Ghia, K.N. Ghia, C.T. Shin, High-resolutions for incompressible flow using the Navier–Stokes equations and a multigrid method, J. Comp. Phys. 48 (1982) 387–411.
[25] D.R. Moore, N.O. Weiss, Two-dimensional Rayleigh–Bénard convection, J. Fluid Mech. 58 (1973) 289–312.
[26] S. Mahmud, P.K. Das, N. Hyder, A.K.M.S. Islam, Free convection in an enclosure with vertical wavy walls, Int. J. Ther. Sci. 41 (2002) 440–446.
[27] T.H. Kuhen, R.J. Goldstein, An experimental and theoretical study of natural convection in the annulus between horizontal concentric cylinders, J. Fluid Mech. 74 (1976) 695–719.
[28] X. Shi, J.M. Khodadadi, Laminar natural convection heat transfer in a differentially heated square cavity due to a thin fin on the hot wall, J. Heat Transfer 125 (2003) 624–634.
[29] S.H. Tasnim, M.R. Collins, Numerical analysis of heat transfer in a square cavity with a baffle on the hot wall, Int. Commun. Heat Mass Transfer 31 (2004) 639–650.
[30] K.L. Walker, G.M. Homsy, Convection in a porous cavity, J. Fluid Mech. 87 (1978) 449–474.
[31] W. Bian, P. Vasseur, E. Bilgen, F. Meng, Effect of an electromagnetic field on natural convection in an inclined porous layer, Int. J. Heat Fluid Flow 17 (1996) 36–44.
[32] S. Mahmud, R.A. Fraser, Magnetohydrodynamic free convection and entropy generation in a square porous cavity, Int. J. Heat Mass Transfer 47 (2004) 3245–3256.
[33] D. Poulikakos, A. Bejan, Natural convection in a porous layer heated and cooled along one vertical side, Int. J. Heat Mass Transfer 27 (1984) 1749–1757.
[34] A. Ben-Nakhi, A.J. Chamkha, Effect of length and inclination of a thin fin on natural convection in a square enclosure, Numer. Heat Transfer (Part A) 50 (2006) 389–407.
[35] A. Benzaoui, X. Nicolas, S. Xin, Efficient vectorized finite-difference method to solve the incompressible Navier–Stokes equation for 3-D mixed-convection flows in high-aspect-ratio channels, Numer. Heat Transfer (Part B) 48 (2005) 277–302.
[36] Y.L. He, W.W. Yang, W.Q. Tao, Three-dimensional numerical study of natural convective heat transfer of liquid in a cubic enclosure, Numer. Heat Transfer (Part A) 47 (2005) 917–934.
[37] A. Andreozzi, B. Buonomo, O. Manca, Numerical study of natural convection in vertical channels with adiabatic extensions downstream, Numer. Heat Transfer (Part A) 47 (2005) 741–762.
[38] H. Ding, C. Shu, K.S. Yeo, Z.L. Lu, Simulation of natural convection in eccentric annuli between a square outer cylinder and a circular

inner cylinder using local MQ-DQ method, Numer. Heat Transfer (Part A) 47 (2005) 291–313.
[39] Y.Y. Yan, H.B. Zhang, J.B. Hull, Numerical modeling of electrohydrodynamic (EHD) effect on natural convection in an enclosure, Numer. Heat Transfer (Part A) 46 (2004) 453–471.
[40] N.O. Moraga, S.A. Vega, Unsteady three-dimensional natural convection of water cooled inside a cubic enclosure, Numer. Heat Transfer (Part A) 45 (2004) 825–839.
[41] J. Niu, Z. Zhu, Numerical evaluation of weakly turbulent flow patterns of natural convection in square enclosure with differentially heated side walls, Numer. Heat Transfer (Part A) 45 (2004) 551–568.
[42] M. Rahman, M.A.R. Sharif, Numerical study of laminar natural convection in inclined rectangular enclosures of various aspect ratios, Numer. Heat Transfer (Part A) 44 (2003) 355–373.
[43] R. Shigemitsu, T. Tagawa, H. Ozoe, Numerical computation for natural convection of air in a cubic enclosure under combination of magnetizing and gravitational forces, Numer. Heat Transfer (Part A) 43 (2003) 449–463.
[44] B.A.K. Abu-Hijleh, Optimization of natural convection heat transfer from a cylinder with high conductivity fins, Numer. Heat Transfer (Part A) 43 (2003) 65–82.
[45] G. Wang, An efficient equal-order finite-element method for natural convection in complex enclosures, Numer. Heat Transfer (Part B) 42 (2002) 307–324.
[46] D.W. Pepper, K.G.T. Hollands, Summary of benchmark numerical studies for 3-D natural convection in an air-filled enclosure, Numer. Heat Transfer (Part A) 42 (2002) 1–11.
[47] R.L. Frederick, O. Berbakow, Natural convection in cubical enclosures with thermal sources on adjacent vertical walls, Numer. Heat Transfer (Part A) 41 (2002) 331–340.
[48] M.F. Baig, A. Masood, Natural convection in a two-dimensional differentially heated square enclosure undergoing rotation, Numer. Heat Transfer (Part A) 40 (2001) 181–202.
[49] C.Y. Han, S.W. Baek, The effects of radiation on natural convection in a rectangular enclosure divided by two partitions, Numer. Heat Transfer (Part A) 37 (2000) 249–270.
[50] B. Abourida, M. Hasnaoui, S. Douamna, Transient natural convection in a square enclosure with horizontal walls submitted to periodic temperature, Numer. Heat Transfer (Part A) 36 (1999) 737–750.
[51] M.Y. Ha, M.J. Jung, Y.S. Kim, Numerical study on transient heat transfer and fluid flow of natural convection in an enclosure with a heat-generating conducting body, Numer. Heat Transfer (Part A) 35 (1999) 415–433.
[52] H.Y. Pak, K.W. Park, Numerical analysis of natural convective and radiative heat transfer in an arbitrary shaped enclosure, Numer. Heat Transfer (Part A) 34 (1998) 553–569.
[53] J.Y. Oh, M.Y. Ha, K.C. Kim, Numerical study of heat transfer and flow of natural convection in an enclosure with a heat generating conducting body, Numer. Heat Transfer (Part A) 31 (1997) 289–303.
[54] Y. Ju, Z. Chen, Numerical simulation of natural convection in an enclosure with discrete protruding heaters, Numer. Heat Transfer (Part A) 29 (1996) 671–689.
[55] S.L. Garrett, Resource letter: TA-1: Thermoacoustic engines and refrigerators, Am. J. Phys. 72 (2004) 11–17.
[56] N. Cao, J.R. Olson, G.W. Swift, S. Chen, Energy flux density in a thermoacoustic couple, J. Acoust. Soc. Am. 99 (1996) 3456–3464.
[57] H. Ishikawa, D.J. Mee, Numerical investigation of flow and energy fields near a thermoacoustic couple, J. Acoust. Soc. Am. 111 (2002) 831–839.
[58] S. Mahmud, R.A. Fraser, An analytical solution and computer simulation for a multi-plate thermoacoustic system, Int. J. Exergy 2 (2005) 207–230.
[59] G.D. Mallinson, G.D.V. Davis, Three-dimensional natural convection in a box: A numerical study, J. Fluid Mech. 83 (1977) 1–31.
[60] T. Bednarz, E. Fornalik, T. Tagawa, H. Ozoe, J.S. Szmyd, Experimental and numerical analyses of magnetic convection of paramagnetic fluid in a cube heated and cooled from opposing vertical walls, Int. J. Ther. Sci. 44 (2005) 933–943.
[61] StarCD/StarWorks, CD-adapco (www.cd-adapco.com), 9401 General Drive (Suite 131), Detroit, MI 48170, USA, 2006.